The gas-liquid transition of the two-dimensional Lennard-Jones fluid

J. Phys.: Condens. Matter **2** (1990) 7009–7032. Printed in the UK

The gas–liquid transition of the two-dimensional Lennard-Jones fluid†

M Rovere‡§, Dieter W Heermann§ and K Binder§

‡ Dipartimento di Fisica Teorica, Università di Trieste, I-34014 Trieste, Italy||
§ Institut für Physik, Johannes Gutenberg Universität Mainz, Staudinger Weg 7, D-6500 Mainz, Federal Republic of Germany

Received 30 November 1989, in final form 15 March 1990

Abstract. Monte Carlo simulations of two-dimensional fluids with a truncated Lennard-Jones interaction in the NVT ensemble are analysed with a block density distribution technique, for $N = 256$ and $N = 576$ particles. It is shown that below T_c (critical temperature) the block density function develops a well defined two-peak structure. From the locations of these two peaks the densities of the two coexisting phases can be reliably estimated. In the one-phase region the width of the single peak is used to extract information on the compressibility, by extrapolating the results for finite block size versus inverse block linear dimension to the thermodynamic limit. Studying the temperature dependence of the fourth-order cumulant of the block density distribution at the critical density for various block sizes, the location of the critical temperature is found from the intersection of the cumulants, just as in the simpler case of Ising models. Our results suggest that finite-size scaling techniques can be used to analyse the critical properties of Lennard-Jones fluids and related systems.

1. Introduction

The calculation of the phase diagrams of fluids from information on intermolecular forces by Monte Carlo or molecular dynamics computer simulation has remained of outstanding interest since the introduction of these techniques [1,2]. Despite very impressive progress (see [3–9] for some recent reviews), it still is a difficult problem, even for a simple fluid, to study the region near the critical point of the gas–liquid transition, and precisely estimate the location of the gas–liquid coexistence curve, characterising the related physical properties (e.g. compressibilities) quantitatively. Although this problem has been considered extensively and various approaches to deal with it have been devised (see e.g. [10–20] for methods successful in conditions away from the critical region), there still is need for additional and complementary approaches.

In the present paper we apply such an approach to the two-dimensional Lennard-Jones fluid. Our method is an extension of finite-size scaling techniques [21–25], which are a standard tool for the analysis of phase transitions of lattice models [3,4,5].

† Work done in collaboration with the Condensed Matter Group of SISSA, Trieste.
|| Present and permanent address.

0953-8984/90/337009+24$03.50

While for a Monte Carlo simulation in the NVT ensemble of a fluid (N being the number of particles, V the total volume of the box and T the temperature) the average density $\rho = N/V$ of the system is strictly constant, we can observe fluctuations of the density in *subsystems*. For a liquid–gas phase transition, the density difference between the liquid and the gas phases is the *order parameter* of the phase transition, and hence the study of the density fluctuations is of key importance in understanding the phase transition. The change in the properties of the density distribution function of subsystem cells contains fairly complete information on the liquid–gas transition. We shall show that the densities of coexisting phases can be estimated reliably from the distribution function. The behaviour of the compressibility [26] and the location of the critical point can also be extracted from the information contained in the distribution functions.

While the spirit of our approach is related to the idea of directly studying phase coexistence between two system cells, a cell being in the fluid state and one in the gas state, which can exchange atoms at constant pressure [19], the distinguishing feature of our approach is the introduction of finite-size scaling concepts which thus allow a systematic study of size effects, which we consider indispensable near a critical point [24]. Our method thus generalises the approach of [21], which there was formulated for a lattice gas (Ising) model, to an off-lattice fluid.

In section 2 we summarise the main general theoretical ideas about the density probability distribution function $P_L(\rho)$ for subsystems of linear dimension L ($L \times L$ in $d = 2$ dimensions or $L \times L \times L$ in $d = 3$ dimensions), which constitute the basis of our approach. Section 3 gives the main facts on our Monte Carlo simulation of the two-dimensional fluid with (truncated) Lennard-Jones interaction, and gives some *raw data* on configurations of the system and the corresponding $P_L(\rho)$. Section 4 discusses the estimation of the coexisting densities at the gas–fluid transition, while section 5 discusses the estimation of the critical point and the compressibility in the one-phase region. Section 6 contains our conclusions and gives an outlook on possible future extensions. In the appendix we work out some predictions based on a simple van der Waals approach, which can be useful for comparison to our numerical results.

2. The density distribution function $P_L(\rho)$ in subsystems

In the statistical mechanics of many body systems it is a familiar concept to divide the system into *cells* or *blocks* of finite dimension L (figure 1). Defining the particle number in the block as N_i, with $\sum_i N_i = N$, the density ρ_i in the ith block becomes

$$\rho_i = N_i/L^d \qquad L = S/M_b \qquad M_b \text{ integer} \tag{1}$$

S being the linear dimension of the total system. Thus $(S/L)^d = M_b^d$ subsystems are studied simultaneously. Note also that in one simulation run we use the same particle configurations to investigate several choices of M_b simultaneously, and thus the study of a single (but large enough) system already allows some estimation of finite-size effects.

We focus attention on the moments of the distribution function

$$\langle \rho^k \rangle = \int \rho^k P_L(\rho)\, \mathrm{d}\rho \tag{2}$$

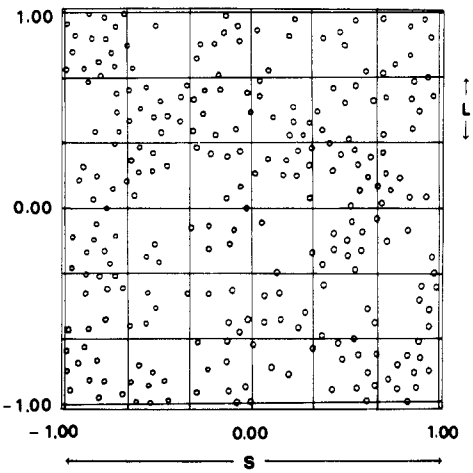

Figure 1. Snapshot picture of the system containing $N = 256$ particles at a reduced density $\rho = 0.3$ (for definitions see section 3) and reduced temperature $T = 0.90$. The cell of total linear size S is divided into blocks of linear dimension $L = S/M_b$, where M_b is an integer. An example for $M_b = 6$ is shown. All lengths in the figure are normalised to $S/2$ and the x,y coordinates of the particles are in the interval $(-1,+1)$. The frame around the cell is for making clear that periodic boundary conditions have been used.

where $P_L(\rho)$ is the average of the density distributions $P_L(\rho_i)$ for $i = 1, \ldots, M_b^d$, i.e. all subsystems are averaged together. The zeroth moment is fixed by normalisation of probabilities and the first moment is of no interest either, since $\langle\rho\rangle = N/V = N/S^d$ is held fixed. The second moment, by standard fluctuation relations [27], is related to the isothermal compressibility K_T

$$\langle(\Delta\rho)^2\rangle_L = \langle(\rho - \langle\rho\rangle)^2\rangle_L = L^{-d}\langle\rho\rangle^2 k_B T K_T^{(L)}. \tag{3}$$

Here our notation emphasises that $K_T^{(L)}$ is the standard isothermal compressibility only in the thermodynamic limit $N \to \infty$ and hence $L \to \infty$, while for small L we expect systematic deviations due to finite-size effects, which will be discussed later.

A useful quantity to be considered is the reduced fourth-order cumulant, which we denote as U_L [21]

$$U_L = 1 - \frac{\langle(\Delta\rho)^4\rangle_L}{3\langle(\Delta\rho)^2\rangle_L^2}. \tag{4}$$

For a state within the one-phase region, the distribution $P_L(\rho)$ is approximately Gaussian if L by far exceeds the correlation length ξ of the order parameter fluctuations (i.e. density fluctuations) [27], $L \gg \xi$

$$P_L(\rho) = L^{d/2}(2\pi\langle(\Delta\rho)^2\rangle)^{-1/2}\exp[-(\Delta\rho)^2/2\langle(\Delta\rho)^2\rangle_L]$$
$$\propto \exp\{-[(\Delta\rho)^2/2\langle\rho\rangle^2][L^d/(k_B T K_T^{(L)})]\}. \tag{5}$$

As is well known, U_L is zero for the Gaussian distribution, (5). Of course, there are corrections to this result since $\langle(\Delta\rho)^4\rangle$ differs from $3\langle(\Delta\rho)^2\rangle_L^2$ by a connected part of a four-particle correlation function. Thus we can write

$$U_L = L^{-d}\chi_l^{(4)}/3K_T^2 \tag{6}$$

where $\chi_l^{(4)}$ tends to a finite non-zero constant as $L \to \infty$. Obviously, $U_L \to 0$ as $L \to \infty$.

The situation is different for a state in a two-phase region where (5) has to be replaced by (again assuming $L \gg \xi$)

$$P_L(\rho) \propto \frac{\rho_{\text{liq}} - \langle\rho\rangle}{\rho_{\text{liq}} - \rho_{\text{gas}}} \frac{1}{\rho_{\text{gas}}(K_T^{\text{gas}})^{1/2}} \exp\left(-\frac{(\rho - \rho_{\text{gas}})^2 L^d}{2\rho_{\text{gas}}^2 k_B T K_T^{\text{gas}}}\right) + \frac{\langle\rho\rangle - \rho_{\text{gas}}}{\rho_{\text{liq}} - \rho_{\text{gas}}} \frac{1}{\rho_{\text{liq}}(K_T^{\text{liq}})^{1/2}} \exp\left(-\frac{(\rho - \rho_{\text{liq}})^2 L^d}{2\rho_{\text{liq}}^2 k_B T K_T^{\text{liq}}}\right). \tag{7}$$

In (7), we have approximated the distribution function as a superposition of two Gaussians centred around the densities ρ_{gas}, ρ_{liq} of the two coexisting phases. The relative weights of the two phases are fixed according to the *lever rule*.

Equation (7) is *not exact* in the limit $L \gg \xi$, since interfacial free energy contributions are neglected [21]. It can be shown in analogy to the arguments presented for lattice gas model that, for $\rho_{\text{gas}} < \rho < \rho_{\text{liq}}$, the decrease of $\ln P_L(\rho)$ is not proportionally to the volume, as suggested by (7)

$$\ln P_L(\rho) \propto -L^d$$

but the leading decay occurs proportionally to the interface area

$$\ln P_L(\rho) \propto -L^{d-1}.$$

Equation (7) is a reasonable starting point for densities ρ in the vicinity of the gas or liquid density, respectively.

We derive (7) from stating that $P_L(\rho)$ in general can be written as (since the subsystems exchange particles, the grand-canonical probability density must be used)

$$P_L(\rho) \propto \exp\{-L^d[f(T,\rho) - \mu\rho]/k_B T\} \tag{8}$$

where $f(T,\rho)$ is the free energy density of the system and μ the chemical potential. Now we can expand $f(T,\rho)$ at $\rho = \rho_{\text{gas}}$ or $\rho = \rho_{\text{liq}}$ quadratically

$$f \simeq f_{\text{gas}} + \mu_{\text{gas}}(\rho - \rho_{\text{gas}}) + \frac{\frac{1}{2}(\rho - \rho_{\text{gas}})^2}{\rho_{\text{gas}}^2 K_T^{\text{gas}}} + \cdots \qquad \rho \simeq \rho_{\text{gas}} \tag{9}$$

$$f \simeq f_{\text{liq}} + \mu_{\text{liq}}(\rho - \rho_{\text{liq}}) + \frac{\frac{1}{2}(\rho - \rho_{\text{liq}})^2}{\rho_{\text{liq}}^2 K_T^{\text{liq}}} + \cdots \qquad \rho \simeq \rho_{\text{liq}}. \tag{10}$$

We must have

$$P_L(\rho) \propto \exp\left(-\frac{(\rho - \rho_{\text{gas}})^2 L^d}{2\rho_{\text{gas}}^2 k_B T K_T^{\text{gas}}}\right) \tag{11}$$

for $\rho \simeq \rho_{\text{gas}}$ and

$$P_L(\rho) \propto \exp\left(-\frac{(\rho - \rho_{\text{liq}})^2 L^d}{2\rho_{\text{liq}}^2 k_B T K_T^{\text{liq}}}\right) \tag{12}$$

for $\rho \simeq \rho_{\mathrm{liq}}$, since for coexisting phases

$$\mu_{\mathrm{gas}} = \mu_{\mathrm{liq}} = \mu_{\mathrm{coex}} \tag{13}$$

and hence

$$f - \mu_{\mathrm{gas}}\rho = f_{\mathrm{gas}} - \mu_{\mathrm{coex}}\rho_{\mathrm{gas}} + \frac{1}{2}\frac{(\rho - \rho_{\mathrm{gas}})^2}{\rho_{\mathrm{gas}}^2 K_T^{\mathrm{gas}}} \tag{14}$$

$$f - \mu_{\mathrm{liq}}\rho = f_{\mathrm{liq}} - \mu_{\mathrm{coex}}\rho_{\mathrm{liq}} + \frac{1}{2}\frac{(\rho - \rho_{\mathrm{liq}})^2}{\rho_{\mathrm{liq}}^2 K_T^{\mathrm{liq}}} = f_{\mathrm{gas}} - \mu_{\mathrm{coex}}\rho_{\mathrm{gas}} + \frac{1}{2}\frac{(\rho - \rho_{\mathrm{liq}})^2}{\rho_{\mathrm{liq}}^2 K_T^{\mathrm{liq}}} \tag{15}$$

involving the double-tangent construction and (13)

$$f_{\mathrm{liq}} = f_{\mathrm{gas}} + \mu_{\mathrm{coex}}(\rho_{\mathrm{liq}} - \rho_{\mathrm{gas}}) \tag{16}$$

and thus the factor $\exp[-(f_{\mathrm{gas}} - \mu_{\mathrm{gas}}\rho_{\mathrm{gas}})L^d/k_{\mathrm{B}}T]$ is a common factor to the probability both at the gas and the liquid side of phase coexistence. For a coexistence of macroscopic regions of gas and liquid phases for $\rho_{\mathrm{gas}} < \rho < \rho_{\mathrm{liq}}$, the chemical potential lies at $\mu = \mu_{\mathrm{coex}}$, and (7) describes the appropriately weighted linear combination of single-phase distribution functions. Clearly, interfacial contributions to $P_L(\rho)$ are neglected, while bulk density fluctuations are taken into account.

For (7) the cumulant, (4), indeed has an interesting non-trivial behaviour, which makes it a suitable quantity if one wishes to distinguish between one-phase regions and two-phase regions. This is already seen in the limit where (7) is simplified further, i.e. by neglecting bulk fluctuations, replacing the Gaussians by δ-functions

$$P_\infty(\rho) = \frac{\rho_{\mathrm{liq}} - \langle\rho\rangle}{\rho_{\mathrm{liq}} - \rho_{\mathrm{gas}}}\delta(\rho - \rho_{\mathrm{gas}}) + \frac{\langle\rho\rangle - \rho_{\mathrm{gas}}}{\rho_{\mathrm{liq}} - \rho_{\mathrm{gas}}}\delta(\rho - \rho_{\mathrm{liq}}). \tag{17}$$

From (17) it is trivial to obtain

$$\langle(\Delta\rho)^2\rangle = \langle\rho\rangle(\rho_{\mathrm{liq}} + \rho_{\mathrm{gas}} - \langle\rho\rangle) - \rho_{\mathrm{liq}}\rho_{\mathrm{gas}} \tag{18}$$

$$\begin{aligned}\langle(\Delta\rho)^4\rangle = {} & -3\langle\rho^4\rangle + 6\langle\rho\rangle^3(\rho_{\mathrm{liq}} + \rho_{\mathrm{gas}}) - 2\langle\rho\rangle^2(2\rho_{\mathrm{gas}}^2 + 5\rho_{\mathrm{gas}}\rho_{\mathrm{liq}} + 2\rho_{\mathrm{liq}}^2) \\ & + \langle\rho\rangle(\rho_{\mathrm{liq}}^3 + 5\rho_{\mathrm{liq}}^2\rho_{\mathrm{gas}} + 5\rho_{\mathrm{liq}}\rho_{\mathrm{gas}}^2 + \rho_{\mathrm{gas}}^3) - \rho_{\mathrm{liq}}\rho_{\mathrm{gas}}(\rho_{\mathrm{gas}}^2 + \rho_{\mathrm{gas}}\rho_{\mathrm{liq}} + \rho_{\mathrm{liq}}^2).\end{aligned} \tag{19}$$

It is convenient to express the moments and the cumulant in terms of the volume fraction x of the liquid phase

$$\langle\rho\rangle = \rho_{\mathrm{gas}} + (\rho_{\mathrm{liq}} - \rho_{\mathrm{gas}})x. \tag{20}$$

This yields

$$\langle(\Delta\rho)^2\rangle = (\rho_{\mathrm{liq}} - \rho_{\mathrm{gas}})^2 x(1 - x) \tag{21}$$

$$\langle(\Delta\rho)^4\rangle = (\rho_{\mathrm{liq}} - \rho_{\mathrm{gas}})^4(x - 4x^2 + 6x^3 - 3x^4) \tag{22}$$

and for the cumulant we get

$$U_\infty = -\frac{6x^2 - 6x + 1}{3x(1-x)}. \tag{23}$$

Now we will discuss this expression further. From (23) it is easy to see that the maximum value, $U_\infty = \frac{2}{3}$, is reached for $x = \frac{1}{2}$, i.e. for $\langle\rho\rangle = (\rho_{\text{gas}} + \rho_{\text{liq}})/2$, the density at the *rectilinear diameter*, while for $x \to 0$ or $x \to 1$, U_∞ diverges to $-\infty$. This sign change of U_∞ occurs for $x_\pm = (1 \pm 1/\sqrt{3})/2$.

The singular behaviour of U_∞ for $\rho = \rho_{\text{gas}}$ or $\rho = \rho_{\text{liq}}$, where U_∞ jumps from 0 to $-\infty$, in a finite system is rounded off, of course. It is clear that replacing (17) by (7) will result in corrections of order L^{-d} to the various moments in (18) and (19). Therefore U_L near $\rho = \rho_{\text{gas}}$ or $\rho = \rho_{\text{liq}}$ reaches only a value of order $-L^d$.

All these considerations apply in the limit $L \gg \xi$ only, as has been emphasised above. Now we are considering the opposite case, $L \leq \xi$, i.e. the vicinity of the critical point. There the distribution function already in the single-phase region is distinctly non-Gaussian. Following the experience with the Ising model [21], we make a scaling assumption, [$\epsilon = 1 - T/T_c$, $\xi \sim |\epsilon|^{-\nu}$]

$$P_L(\rho) = L^{\beta/\nu}\tilde{P}\{(\rho - \rho_c)L^{\beta/\nu}, (\langle\rho\rangle - \rho_c)|\epsilon|^{-\beta}, L|\epsilon|^{\nu}\}. \tag{24}$$

Here β and ν are the critical exponents of the order parameter and correlation length, respectively, and ρ_c is the critical density, T_c the critical temperature. The scaling function $\tilde{P}(x, y, z)$ does not need to be specified explicitly at this point. From (24) we conclude

$$\langle(\Delta\rho)^2\rangle = L^{-2\beta/\nu} f_2\{(\langle\rho\rangle - \rho_c)|\epsilon|^{-\beta}, L|\epsilon|^{\nu}\} \tag{25}$$

$$\langle(\Delta\rho)^4\rangle = L^{-4\beta/\nu} f_4\{(\langle\rho\rangle - \rho_c)|\epsilon|^{-\beta}, L|\epsilon|^{\nu}\} \tag{26}$$

$$U_L = f_u\{(\langle\rho\rangle - \rho_c)|\epsilon|^{-\beta}, L|\epsilon|^{\nu}\} \tag{27}$$

where f_2, f_4 and f_u are scaling functions. Equations (3) and (25), together with the scaling relation $\gamma + 2\beta = d\nu$ for the compressibility exponent, imply the finite-size scaling expression for the compressibility

$$K_T^{(L)} = L^{\gamma/\nu}(\langle\rho\rangle^2 k_B T)^{-1} f_2\{(\langle\rho\rangle - \rho_c)|\epsilon|^{-\beta}, L|\epsilon|^{\nu}\}. \tag{28}$$

Of particular interest for us is the case $\langle\rho\rangle = \rho_c$, where the scaling functions f_2, f_4 and f_u have only a single argument $L|\epsilon|^{\nu}$. In this case the finite-size scaling technique, well established in the simulation of lattice models [3–6, 21–25], can be carried over straightforwardly. In particular, the cumulants U_L for different values of L must intersect in a common intersection point $U^* = f_u(0, 0)$. Locating such an intersection point can be used as a criterion to find T_c. Of course the situation is much more complicated than for the lattice gas model, where $\rho_c = \frac{1}{2} = \frac{1}{2}(\rho_{\text{gas}} + \rho_{\text{liq}})$ holds exactly, since ρ_c for off-lattice models is not exactly known in general, and also $\rho_c \neq \frac{1}{2}(\rho_{\text{gas}} + \rho_{\text{liq}})$ for $T < T_c$. Thus a criterion to locate ρ_c is also needed. For this purpose, we note that the functions f_2 and f_u should have their maximum for $\langle\rho\rangle = \rho_c$, e.g., for $T = T_c$ we expect a behaviour

$$U_L = \tilde{U}\{(\langle\rho\rangle - \rho_c)L^{\beta/\nu}\} \tag{29}$$

where $\tilde{U}(0) = U^*$, while $\tilde{U}(x \gg 1) \sim (\langle\rho\rangle - \rho_c)^{-d\nu/\beta} L^{-d}$, cf (6). Checking for the scaling described by (29) is a test that ρ_c has been correctly found.

Our analysis implies that for $\langle\rho\rangle = \rho_c$, upon lowering the temperature, above T_c, the cumulant U_L increases from very small values proportional to L^{-d} (6) up to a universal value U^* at T_c. This value is the same as is observed in the Ising (lattice gas) model at the same dimensionality. For T slightly below T_c, U_L reaches its maximum positive value, $U_{L\to\infty} = \frac{2}{3}$, and then it decreases again. U_L approaches the value U_∞ given in (23), but x differs more and more from $x = \frac{1}{2}$ as the temperature is lowered, due to the increased difference between ρ_c and $\frac{1}{2}(\rho_{liq} + \rho_{gas})$. Thus the temperature variation of U_L is not a monotonic increase with decreasing temperature, as it is in the lattice gas model for $\rho_c = \frac{1}{2}$.

In practice the simulations consider rather small block sizes L, where many of the relations written down here are not yet strictly valid. The relations (24)–(29) are valid only in the limit $L \to \infty$, $\xi \to \infty$, L/ξ finite, and disregard corrections to finite-size scaling. Likewise, also for $L \gg \xi$, where (5) and (7) are supposed to hold, the *effective* compressibility $K_T^{(L)}$ defined from either the second moment of the density fluctuation in a subblock (3), or from the half width of the distribution (5) will differ from the physical compressibility $K_T \equiv K_T^{(\infty)}$, resulting in the thermodynamic limit. To leading order, we expect that K_T and $K_T^{(L)}$ differ by a boundary correction

$$K_T^{(L)} = K_T[1 - \text{constant}\,(\xi/L)] \qquad L \gg \xi. \tag{30}$$

The justification for (30) comes from comparing the microscopic definitions

$$\langle\rho\rangle^2 k_B T K_T^{(L)} = \frac{1}{L^d} \int_{\text{cell}} d\boldsymbol{r} \int_{\text{cell}} d\boldsymbol{r}' \,\langle[\rho(\boldsymbol{r}) - \langle\rho\rangle][\rho(\boldsymbol{r}') - \langle\rho\rangle]\rangle \tag{31}$$

and

$$\langle\rho\rangle^2 k_B T K_T = \frac{1}{L^d} \int_{\text{cell}} d\boldsymbol{r} \int d\boldsymbol{r}' \,\langle[\rho(\boldsymbol{r}) - \langle\rho\rangle][\rho(\boldsymbol{r}') - \langle\rho\rangle]\rangle \tag{32}$$

where the second integral in (32) is extended to the total volume. The integrand in both (31) and (32) is zero except if the points $\boldsymbol{r}$, $\boldsymbol{r}'$ are not much farther apart than a distance ξ (with $\xi \ll L$). Now it is clear that for points $\boldsymbol{r}$ close to the wall boundary also correlations $\langle[\rho(\boldsymbol{r}) - \langle\rho\rangle][\rho(\boldsymbol{r}') - \langle\rho\rangle]\rangle$ contribute to (32), where $\boldsymbol{r}'$ is outside the cell ($\boldsymbol{r}'$ must lie in a region of width ξ adjacent to the boundary of the cell). These contributions are missing from (31). Thus the difference between (31) and (32) should be due to a surface to volume ratio, i.e. a factor ξ/L, as anticipated in (30).

3. Monte Carlo results

The simulations were performed for a two-dimensional fluid with a pairwise Lennard-Jones potential

$$v(r) = 4\epsilon\left[\left(\frac{\sigma}{r}\right)^{12} - \left(\frac{\sigma}{r}\right)^{6}\right] \tag{33}$$

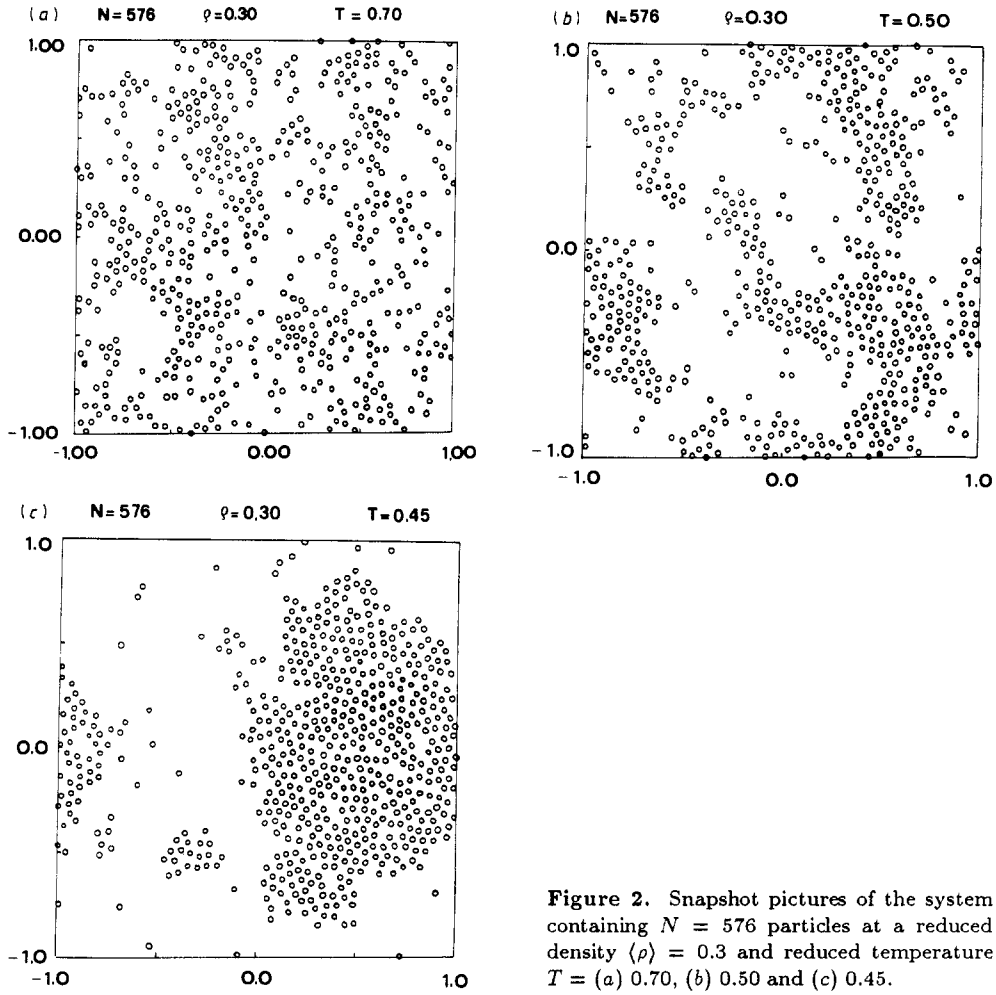

Figure 2. Snapshot pictures of the system containing $N = 576$ particles at a reduced density $\langle\rho\rangle = 0.3$ and reduced temperature $T =$ (*a*) 0.70, (*b*) 0.50 and (*c*) 0.45.

truncated at $r = 2.5\sigma$. We used systems with $N = 256$ and $N = 576$ particles in a box of quadratic shape ($S \times S$) and periodic boundary conditions. Standard Metropolis Monte Carlo methods [1,3–7] were used, applying the NVT ensemble.

Since in the vicinity of the liquid–gas transition we have to expect very strong and *long-lived* density fluctuations, it is not *a priori* clear that an analysis along the lines of section 2 is practically convenient with a reasonable effort in computing time. Therefore we decided to work with small values of N, since this ensures that proper equilibration of the system is always possible for all densities and temperatures, in spite of critical slowing down. A definitive study of the immediate neighbourhood of the critical point must choose much larger N than chosen here. We defer such a study to a later stage of this project, while the present work has the character of a feasibility study.

The strong density fluctuations are already apparent from the *snapshot pictures* of system configurations (figure 2). Here and in the following the density is measured in units of σ^2 and the temperature is measured in units of ϵ/k_B. The density $\langle\rho\rangle = 0.3$, shown in figure 2, is close to the critical density, and $T = 0.5$ is close to the critical temperature. Already in figure 2(*a*) we see strong density fluctuations but their typical

length scale ξ clearly is much less than the box size, ξ is comparable to the box size in the case of figure 2(*b*), and figure 2(*c*) corresponds to a distinctly phase-separated state, where a large liquid droplet coexists with a low-density gas region.

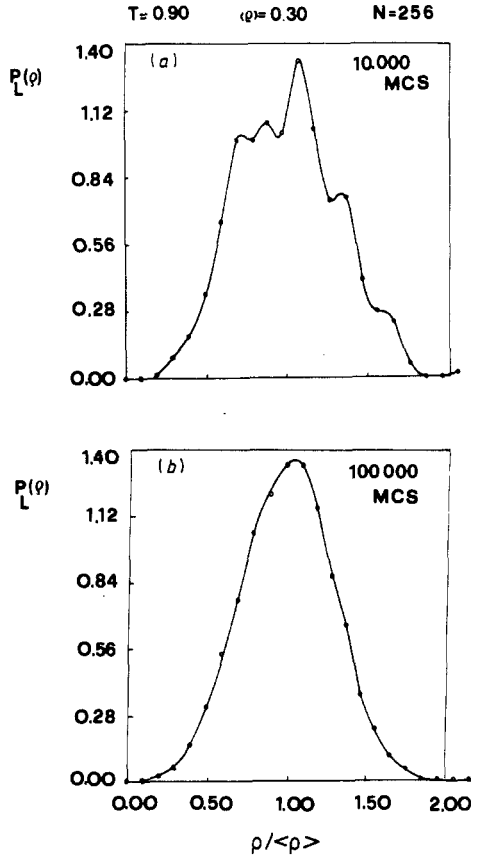

Figure 3. Probability distribution $P_L(\rho)$ for $N = 256$, $T = 0.90$, $\langle\rho\rangle = 0.30$ and $M_b = 5$ ($L = S/M_b$), after taking averages over (*a*) 10 000 MCS and (*b*) 100 000 MCS.

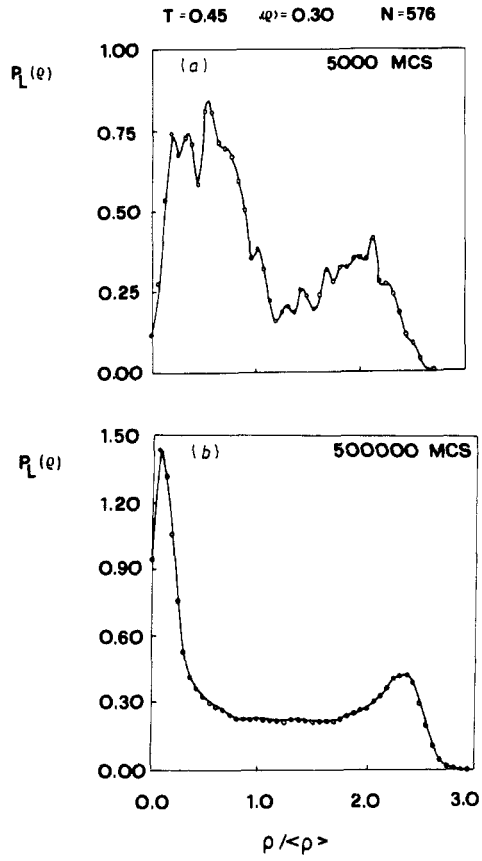

Figure 4. Probability distribution $P_L(\rho)$ for $N = 576$, $T = 0.45$, $\langle\rho\rangle = 0.30$ and $M_b = 6$, after taking averages over (*a*) 5000 MCS and (*b*) 500 000 MCS.

Starting from a configuration of particles ordered in a square lattice, a number of Monte Carlo runs were performed in order to *melt* the system. Then up to 10^6 Monte Carlo steps (MCS)/particle were used to thermalise the system at the temperature and density, where we want to perform averages. This large effort in equilibration was found necessary, since otherwise long-wavelength Fourier components of the density still were out of equilibrium, and hence some features of $P_L(\rho)$ for large L systematically in error.

Similarly, a large statistical effort is needed in order to sample the density probability distribution $P_L(\rho)$ reliably (figures 3 and 4). This function is not recorded at each MCS, but after a sampling one gives *time* for the particles to diffuse out of the initial subblock; in fact the statistics for the larger block sizes is worse than for smaller block sizes. If one takes a sample of the order of 10^4 MCS/particle only, $P_L(\rho)$ still exhibits a lot of spurious structure, and a reliable moment analysis is not possible. While far above T_c in the one-phase region an effort of about 10^5 MCS/particle is

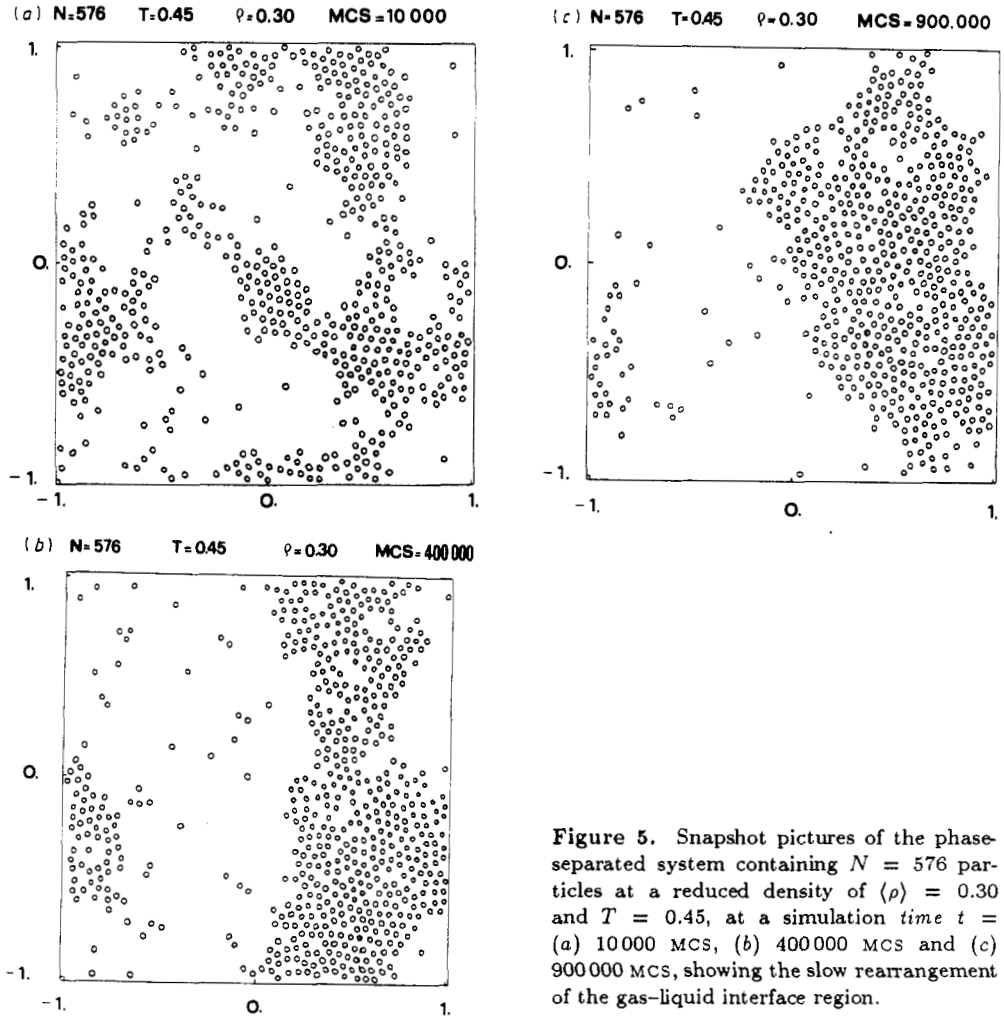

Figure 5. Snapshot pictures of the phase-separated system containing $N = 576$ particles at a reduced density of $\langle\rho\rangle = 0.30$ and $T = 0.45$, at a simulation *time* $t =$ (*a*) 10 000 MCS, (*b*) 400 000 MCS and (*c*) 900 000 MCS, showing the slow rearrangement of the gas–liquid interface region.

sufficient to obtain a well-behaved $P_L(\rho)$, see figure 3, this effort still is not enough in the two-phase coexistence region, where we found it is necessary to use at least 5×10^5 MCS/particle (figure 4). This is expected due to the slow relaxation of the interface region between liquid and gas (figure 5). We present such details of the analysis as a warning against too hasty a conclusion. In figure 4(*a*) the distribution averaged over 10^4 MCS/particle has a reasonable looking two-peak structure, and so one might be misled to stop the simulation there: only much longer runs reveal that the peak positions after 10^4 MCS/particle are not yet at their right place, nor are the peak heights, see figure 4(*b*). Of course, such difficulties are expected in view of the difficulties familiar from the study of first-order transitions [28,29,30] and phase coexistence [31] in lattice models.

However, if these problems are understood, it is feasible to obtain meaningful estimates for the probability distribution $P_L(\rho)$ at various temperatures and block sizes. The examples collected in figure 6 show that the expected gradual change from a Gaussian distribution at temperatures far above criticality to a double-peak distribution below the critical point is clearly seen.

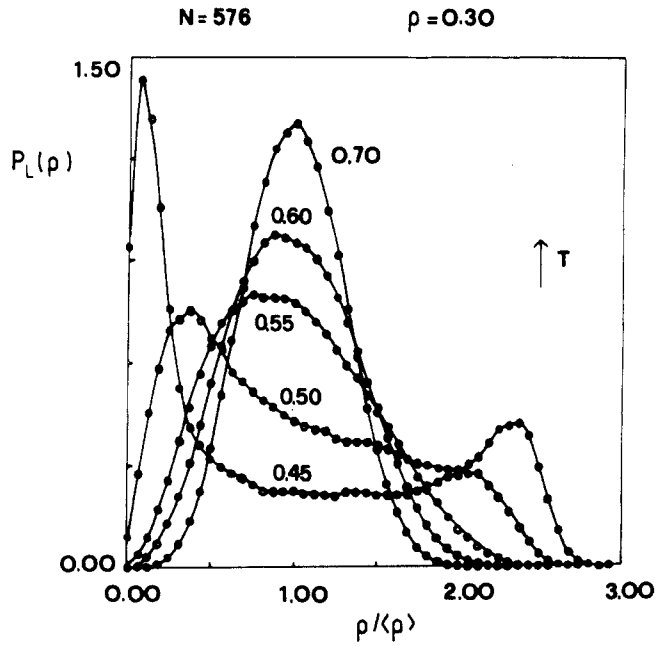

Figure 6. Probability distribution $P_L(\rho)$ plotted versus $\rho/\langle\rho\rangle$ for $N = 576$, $\langle\rho\rangle = 0.30$ and $M_b = 6$. Various temperatures are shown as indicated in the figure.

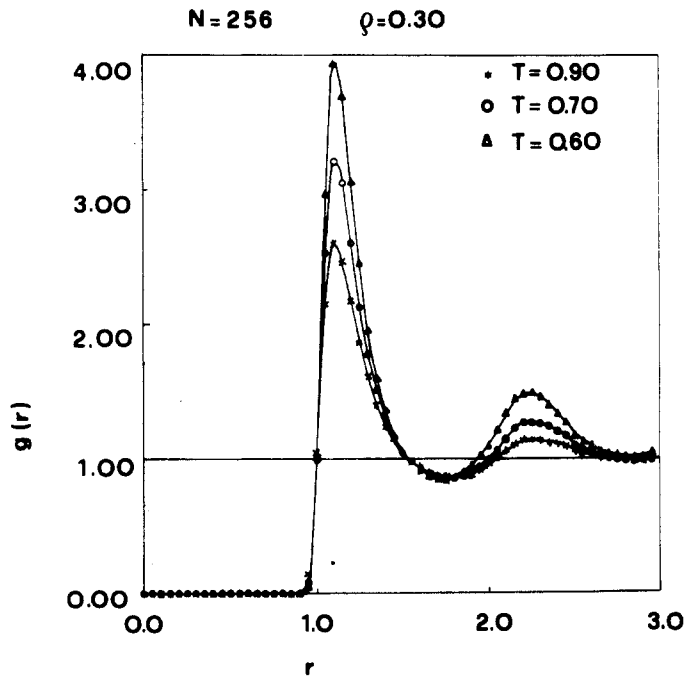

Figure 7. Radial distribution function $g(r)$ plotted versus r (in units of σ) for $N = 256$, $\langle\rho\rangle = 0.30$ and $T = 0.90, 0.70, 0.60$.

Table 1. Internal energy per particle in reduced units (the kinetic contribution is not included) for different values of density and temperature. The values are for the truncated potential without any long-range corrections.

		T			
N	ρ	0.90	0.70	0.60	0.55
256	0.25	−0.749	−0.880	−1.011	
256	0.30	−0.873	−1.008	−1.145	
576			−1.007	−1.146	−1.272
256	0.32	−0.922	−1.055	−1.194	
576			−1.058	−1.195	−1.322
256	0.34	−0.971	−1.101	−1.237	
576			−1.106	−1.245	−1.387
256	0.36	−1.018	−1.150	−1.278	
576			−1.154	−1.283	
256	0.38	−1.068	−1.197	−1.316	
256	0.40	−1.115	−1.240	−1.363	

Table 2. Pressure (in reduced units) for different values of density and temperature. The values are for the truncated potential without any long-range corrections.

		T			
N	ρ	0.90	0.70	0.60	0.55
256	0.25	0.236	0.172	0.134	
256	0.30	0.266	0.202	0.156	
576			0.202	0.156	0.128
256	0.32	0.286	0.214	0.164	
576			0.214	0.164	0.134
256	0.34	0.308	0.228	0.172	
576			0.230	0.174	0.144
256	0.36	0.332	0.242	0.182	
576			0.244	0.182	
256	0.38	0.356	0.258	0.190	
256	0.40	0.382	0.276	0.200	

The analysis of such distribution functions along the lines suggested in section 2 is the main content of the present paper and will be presented in sections 4 and 5. At this point we note, however, that all the quantities traditionally recorded in Monte Carlo simulations of fluids (radial pair distribution functions, internal energy, pressure etc.) can be (and have been) obtained with high accuracy from the same simulation runs that yield $P_L(\rho)$. Figure 7 presents the radial distribution function $g(r)$ at $\rho = 0.3$ and $T = 0.9$, 0.7, 0.6 as an example. In principle, an analysis of $g(r)$ could yield useful information on the correlation length ξ near T_c. Since the sizes of our total box are still quite small, and the behaviour of $g(r)$ at large distances is distorted due to the periodic boundary condition, no such analysis has been attempted here. In tables 1 and 2 we present some of the results for the internal energy and the pressure, as calculated from the virial theorem, in the region of the ρ–T plane which is of interest in the present work. We note that the lack of finite-size effects on energy and pressure for $T \geq 0.6$ should not be taken as indicating that all size effects are small!

4. Estimation of the coexisting densities at the gas–liquid transition

Equation (7) expresses the idea that $P_L(\rho)$ in the two-phase region is a weighted average of two Gaussian peaks, which are centred at ρ_{gas} and ρ_{liq}, irrespective of the average density $\langle\rho\rangle$. Only the relative weights of the two peaks change when $\langle\rho\rangle$ changes at constant T (for $\rho_{\text{gas}} < \langle\rho\rangle < \rho_{\text{liq}}$ of course). Figure 8 shows that this property indeed is nicely established. It is also seen, as expected, that in between the two peaks the distribution shows distinctly non-Gaussian features. The rather large values of $P_L(\rho)$ encountered there should be attributed to contributions from interfacial regions.

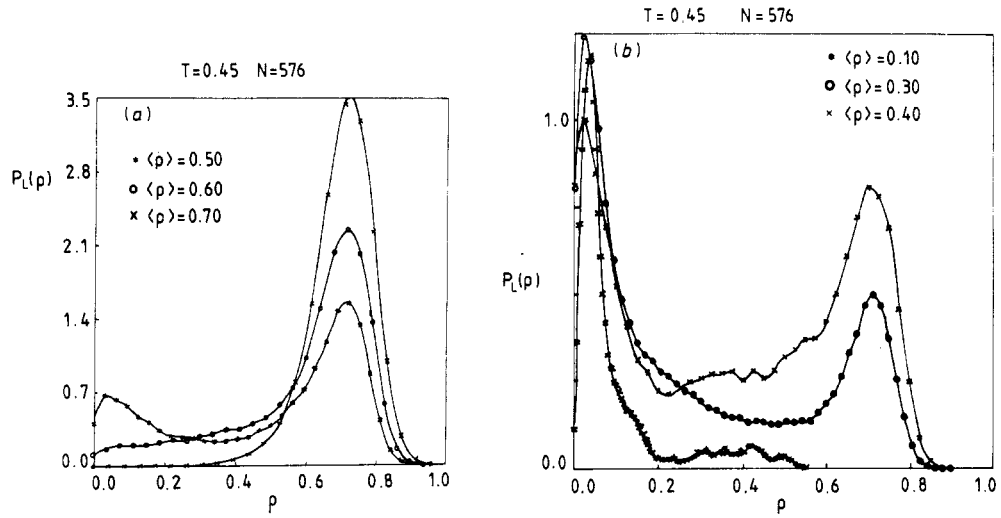

Figure 8. Probability distribution $P_L(\rho)$ plotted versus ρ for $N = 576$, $T = 0.45$, $M_b = 6$, and several choices for $\langle\rho\rangle$: (a) includes $\langle\rho\rangle = 0.50$, 0.60 and 0.70; ($b$) includes $\langle\rho\rangle = 0.10$, 0.30, 0.40.

A primary objective of the present work is to devise a convenient method by which the densities ρ_{gas} and ρ_{liq} of the coexisting phases can be estimated. In order to use data such as shown in figure 8 for this purpose, the dependence of the distribution on block size L and on particle number N must be studied (figure 9). Let us choose $T = 0.45$ and $\langle\rho\rangle = 0.3$. It is seen that for $N = 576$ the gas density settles down at a value $\rho_{\text{gas}} \simeq 0.021$, the liquid density at $\rho_{\text{liq}} \simeq 0.717$. For $N = 256$ the liquid density seems to be somewhat smaller, namely $\rho_{\text{liq}} \simeq 0.684$. Since in this case the minimum in between the two peaks is much shallower, we consider the latter value as less reliable. Hence at this temperature (which is about 10 per cent less than T_c) we are able to estimate ρ_{gas} and ρ_{liq} with accuracies of about one per cent. Choosing a larger value of N would certainly allow us to improve this accuracy substantially, but requires distinctly more effort in computing time in order to equilibrate the system.

In principle, our technique should also allow one to extract estimates for the compressibilities K_T^{gas} and K_T^{liq} at the gas and liquid branches of the coexistence curve, by estimating the widths of the peaks describing the two coexisting phases (7). In practice, the situation is less satisfactory. On the gas side, the peak is too close to zero

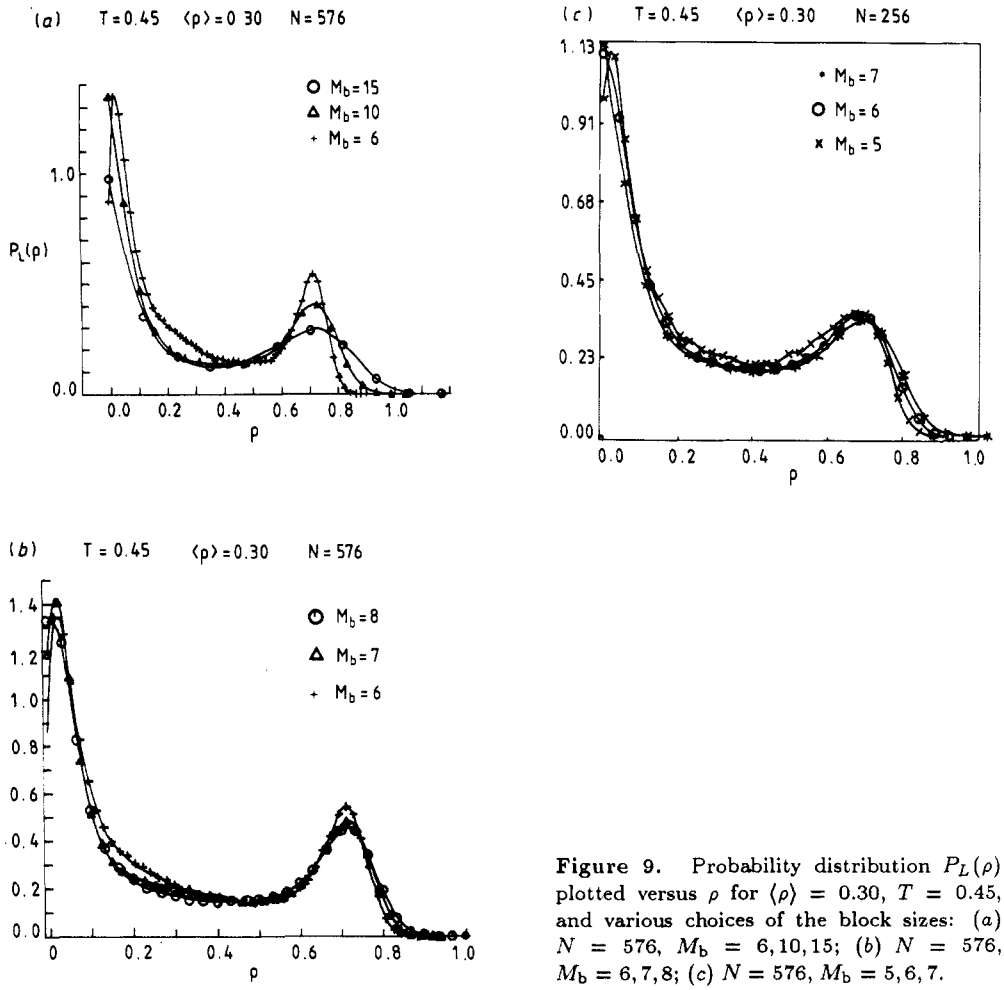

Figure 9. Probability distribution $P_L(\rho)$ plotted versus ρ for $\langle\rho\rangle = 0.30$, $T = 0.45$, and various choices of the block sizes: (*a*) $N = 576$, $M_b = 6,10,15$; (*b*) $N = 576$, $M_b = 6,7,8$; (*c*) $N = 576$, $M_b = 5,6,7$.

density (at least in the example at $T = 0.45$ studied here) and therefore the peak shape is so distorted (note the large entry of $P_L(\rho = 0)$ that is due to blocks which do not contain any atoms at all!) that we consider the estimate for the width fairly unreliable. The analysis of the width of the peaks in figure 8 and 9 is also difficult because of the fact that those blocks that contain pieces of the interfacial region between liquid-like clusters and gas-like regions give rise to densities in between the peaks; therefore these peaks have a distinctly non-Gaussian shape: they are not symmetric with respect to their peak position, ρ_{liq} or ρ_{gas}, respectively. Thus we have used only the part of the distribution for densities exceeding ρ_{liq} to estimate the halfwidth. Table 3 shows that the resulting data are still quite strongly fluctuating, and the plot of $L^2\langle(\Delta\rho)^2\rangle$ versus $1/L$ (this linear extrapolation is suggested by (30)) would be very irregular, making the extrapolation impossible. However, the rough order of magnitude can be estimated.

Probably it is better to estimate K_T^{gas} by appropriate analytical techniques such as thermodynamic perturbation theory [11]. For simplicity, we have only attempted to estimate the order of magnitude of K_T by using the van der Waals equation inserting the observed value for ρ into it (see the appendix). Of course, this procedure cannot

be quantitatively correct, since the true shape of the coexistence curve near T_c is characterised by a critical exponent $\beta = \frac{1}{8}$ rather than the van der Waals value $\beta = \frac{1}{2}$. Table 3 reveals, however, that the estimates from the simulation are about a factor 15 larger than the estimate from the van der Waals equation, which hence probably is too crude an approximation to estimate the order of magnitude of K_T correctly [32].

At this temperature the virial expansion up to the fourth-order term gives a value for the gas density at coexistence that is too low (of the order of 0.005), the reason perhaps being that the virial expansion gives $T_c \simeq 0.49$ but a critical density that is too small ($\rho \simeq 0.119$) [33]. For the compressibility one cannot get better results in comparison with the van der Waals equation.

However, from a more sophisticated analysis of virial expansions combined with previous simulations (Reddy and O'Shea [34]) we obtain $\rho_{gas} \simeq 0.029$ and $\rho_{liq} \simeq 0.727$ in good agreement with the present work.

Table 3. Liquid density ρ_{liq} and normalised isothermal compressibility $k_B T \rho_{liq} K_T^{liq}$ for $T = 0.45$, $N = 576$, $\langle\rho\rangle = 0.3$ at the liquid branch of the coexistence curve, for different values of the parameter M_b controlling the subblock size. Using $\rho_{liq} = 0.72$ in the van der Waals equation for $\rho_c = 0.30$, $T/T_c = 0.9$ would yield $k_B T \rho_{liq} K_T^{liq} \simeq 0.0526$, while use of the van der Waals prediction $\rho_c \simeq 0.50$ for those parameters would yield $k_B T \rho_{liq} K_T^{liq} \simeq 1.116$.

M_b	ρ_{liq}	$k_B T \rho_{liq} K_T^{liq}$
6	0.711	0.867
7	0.718	0.763
8	0.720	0.730
9	0.718	0.814
10	0.719	0.753
11	0.718	0.875
12	0.698	1.169
13	0.715	0.828
14	0.722	0.830
15	0.715	1.057

5. Estimation of the critical point and the compressibility in the one-phase region

Figure 10 shows the probability distribution $P_L(\rho)$ for $N = 256$ and $T = 0.9, 0.55$ and $T = 0.50$, respectively, while figure 11 shows data for $N = 576$ at $T = 0.7, 0.55$ and 0.50 (data for $T = 0.7, N = 256$ can be found in [26]).

These curves show the crossover from the Gaussian behaviour of the distribution for $L \gg \xi$ to non-Gaussian behaviour in the critical region ($L \simeq \xi$). Applying (3) to these distributions we can obtain $K_T^{(L)}$. Since there are huge statistical fluctuations, runs typically were extended over up to 800 000 MCS/particle. Due to the smallness of N the divergence of the relaxation time near the critical point (*critical slowing down*) is rounded off. 800 000 MCS/particle seems to suffice even in the critical region. However, the size dependence of $K_T^{(L)}$, which is linear in $1/L$ at high temperature (figure 12(*a*)) as expected (30), becomes non-trivial in the critical region (figures 12(*b*) and 12(*c*)). Then a meaningful extrapolation to the thermodynamic limit becomes

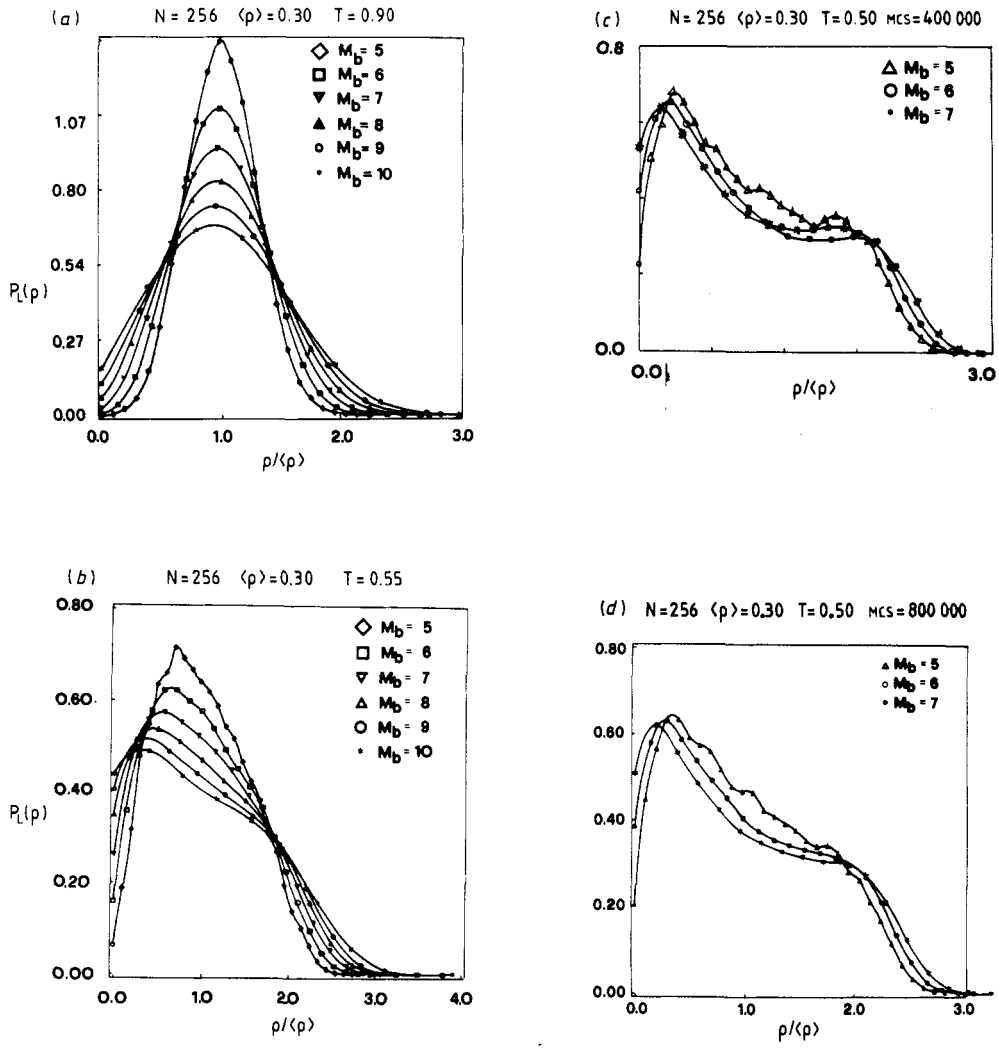

Figure 10. Probability distribution $P_L(\rho)$ plotted versus ρ for $\langle\rho\rangle = 0.30$, $N = 256$, various temperatures and block sizes: (*a*) $T = 0.90$, $M_b = 5,6,7,8,9,10$; (*b*) $T = 0.55$, $M_b = 5,6,7$; (*c*) $T = 0.50$, $M_b = 5,6,7$, after an average of 400 000 MCS; (*d*) same as (*c*) but after 800 000 MCS.

difficult. Of course, this problem is not specific to the Lennard-Jones fluid, it occurs for the Ising lattice gas as well (cf figure 5 of [21]). Thus a finite-size scaling analysis based on (28) needs to be used. A serious problem, however, is that the analysis presented in section 2 really presupposes that subsystems of an *infinite* system are available, while the actual subsystems refer to a system of rather small total number of particles, N. Figure 13 shows that this caveat is relevant at rather high temperatures already. At $T = 0.70$ size effects on the extrapolated values of $K_T/K_T^{(0)}$ are clearly apparent and distinctly more pronounced than size effects on internal energy (table 1) or pressure (table 2). This should not come as a surprise. While internal energy and pressure are dominated by short-range density correlations, K_T is sensitive against

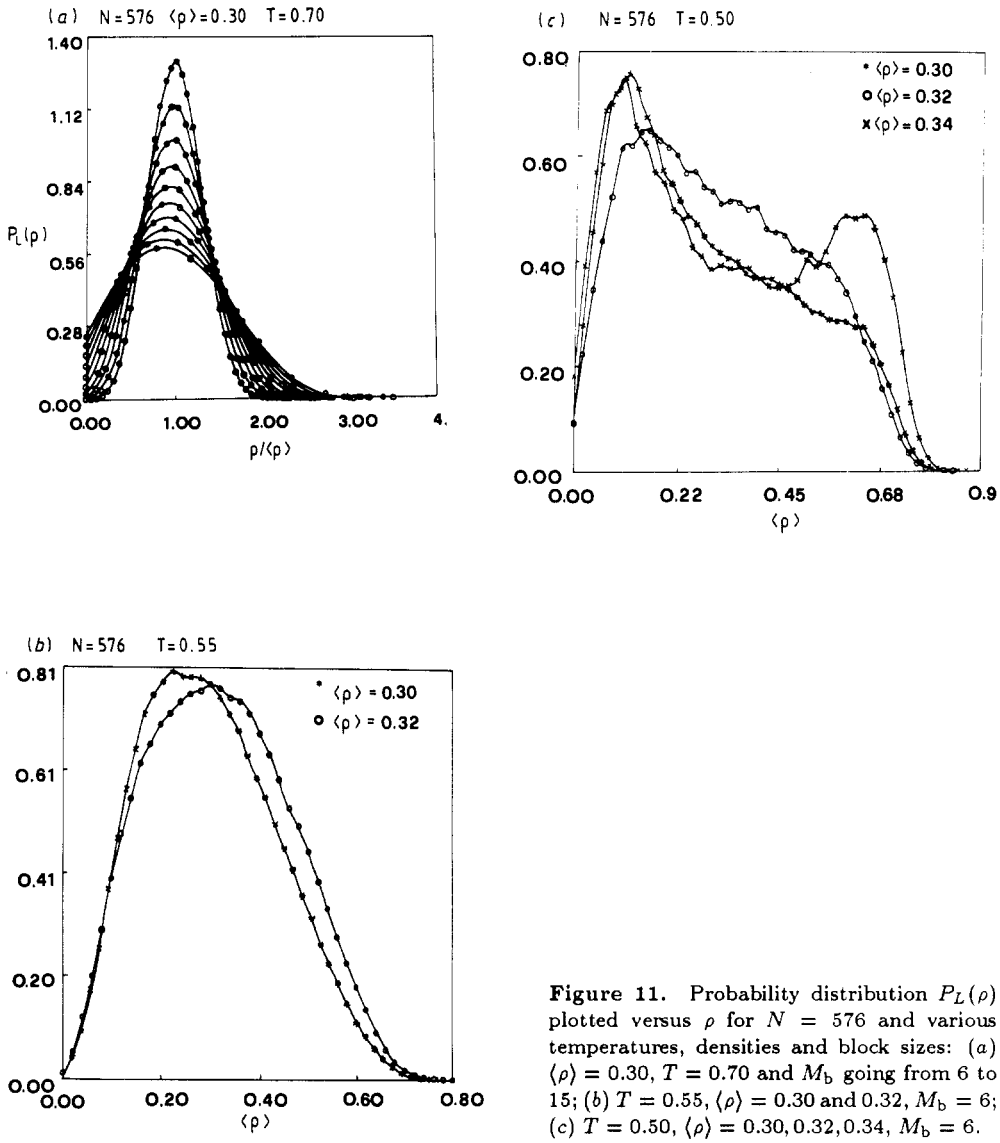

Figure 11. Probability distribution $P_L(\rho)$ plotted versus ρ for $N = 576$ and various temperatures, densities and block sizes: (*a*) $\langle\rho\rangle = 0.30$, $T = 0.70$ and M_b going from 6 to 15; (*b*) $T = 0.55$, $\langle\rho\rangle = 0.30$ and 0.32, $M_b = 6$; (*c*) $T = 0.50$, $\langle\rho\rangle = 0.30, 0.32, 0.34$, $M_b = 6$.

long-range density correlations, cf (32), and the growth of these correlations (which ultimately become critical at T_c) already sets in far above T_c. In order to obtain high-precision estimates of K_T, it seems indispensable to perform runs at still larger values of N and make sure that the data converge to a well defined N-independent limit.

Since such a study is very demanding with respect to computer resources (for larger N also critical slowing down becomes more and more of a problem) we have not attempted to do this yet, but address the question of whether one can obtain meaningful estimates for the critical temperature, using the cumulant analysis of section 2. Figure 14(*a*) reveals the expected trends. In the one-phase region ($T = 0.70, 0.60, 0.55$), the values of U_L are quite small, and also decrease with increasing block size (note that the largest block sizes are least reliable, since the statistics is worst and effects due

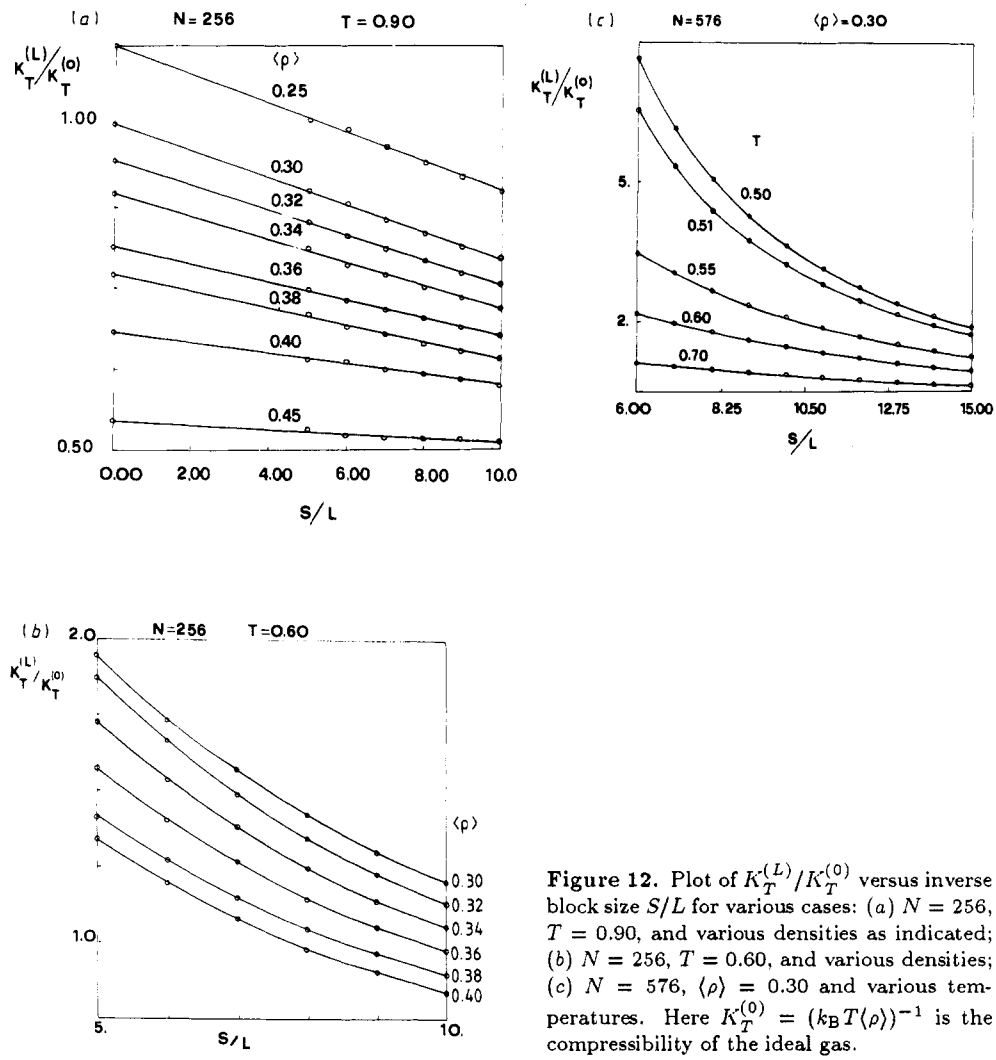

Figure 12. Plot of $K_T^{(L)}/K_T^{(0)}$ versus inverse block size S/L for various cases: (*a*) $N = 256$, $T = 0.90$, and various densities as indicated; (*b*) $N = 256$, $T = 0.60$, and various densities; (*c*) $N = 576$, $\langle\rho\rangle = 0.30$ and various temperatures. Here $K_T^{(0)} = (k_B T\langle\rho\rangle)^{-1}$ is the compressibility of the ideal gas.

to the finiteness of N introduce systematic errors). At low temperatures ($T = 0.45$), U_L is quite large and increases with increasing L. Since $\langle\rho\rangle = 0.3$ for $T = 0.45$ is not at the density of the rectilinear diameter $\frac{1}{2}(\rho_{\text{gas}} + \rho_{\text{liq}}) \simeq 0.37$, U_L does not approach the maximum positive value $U_\infty = 2/3$, but settles down at a distinctly smaller value, which according to (23) should be about $U_\infty = 0.61$ (taking $x \simeq 0.4$). Probably N is too small to have $L \gg \xi$ at $T = 0.45$, even for the largest subblocks, and therefore it is not possible to see the data approaching that value. It is reassuring that for $\langle\rho\rangle = 0.4$, a value closer to $(\rho_{\text{gas}} + \rho_{\text{liq}})/2$, where according to (23) $U_\infty = 0.65$, distinctly larger values of U_L at $T = 0.45$ are obtained throughout (figure 14(*b*)).

In the vicinity of the critical point the curve U_L versus S/L is very flat, and should reach values close to the expected universal value $U^* = 0.52$ [35]. In fact, figure 14 has a striking qualitative similarity to the corresponding data in the Ising model (see figure 12(*a*) of [21]), apart from the fact that the lattice gas calculation of [22] was carried out in the grand-canonical ensemble, where, rather than (23), $U_\infty = \frac{2}{3}$ for $T < T_c$ at $\mu = \mu_{\text{coex}}$, the value at the coexistence curve. Moreover, in the grand-

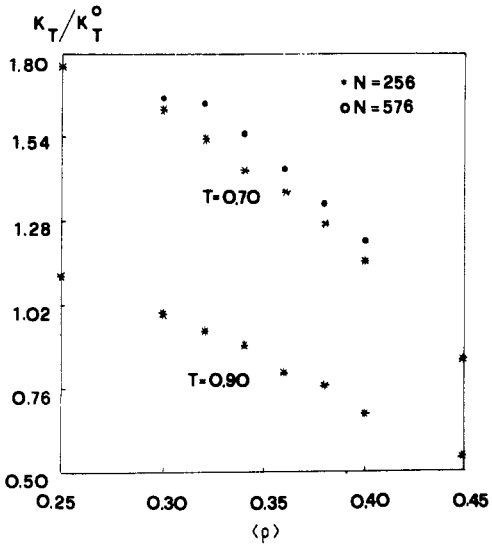

Figure 13. Extrapolated values $K_T^{(L\to\infty)}/K_T^{(0)}$ of the normalised compressibility plotted versus density at $T = 0.70$ and $T = 0.90$ as indicated. At $T = 0.70$ both the results for $N = 256$ and $N = 576$ are included.

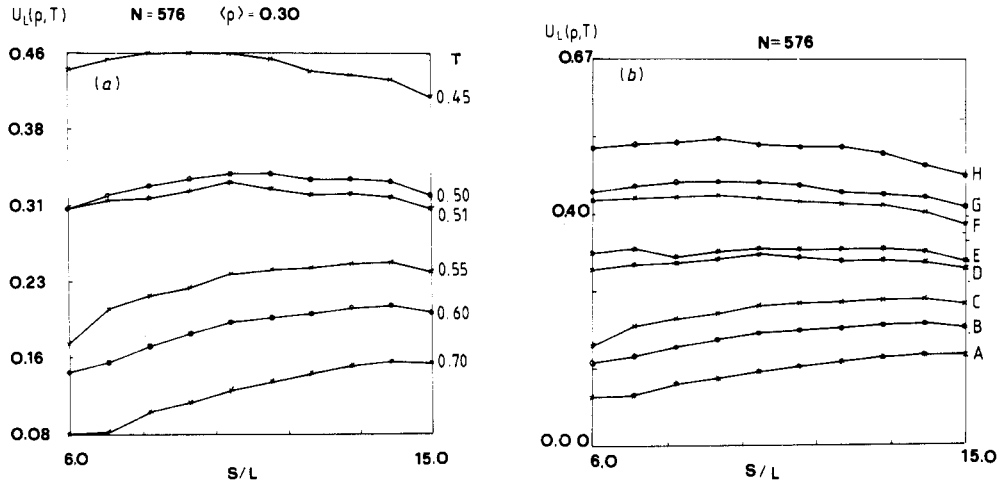

Figure 14. (*a*) Cumulant U_L plotted versus $M_b = S/L$ for $N = 576$ and various temperatures at $\langle\rho\rangle = 0.30$, and (*b*) for several temperatures and various densities $(T, \langle\rho\rangle)$: $A = (0.70, 0.30)$, $B = (0.60, 0.30)$, $C = (0.55, 0.30)$, $D = (0.51, 0.30)$, $E = (0.52, 0.32)$, $F = (0.50, 0.34)$, $G = (0.45, 0.30)$, $H = (0.45, 0.40)$.

canonical ensemble the calculation is neither affected by phase coexistence effects, nor by interfacial contributions, while the latter are probably pronounced in the data presented here.

It is also important to note that near T_c the U_L versus $1/L$ curves are not only flat for $\langle\rho\rangle = 0.3$ but also for neighbouring densities, e.g. $\langle\rho\rangle = 0.32$ or 0.34 (figure 14(*b*)).

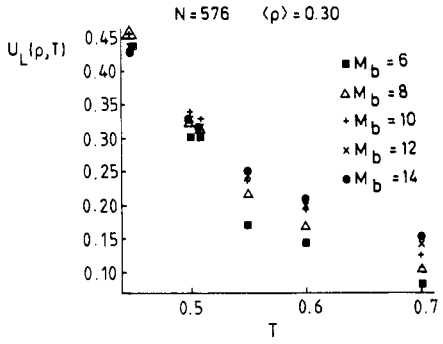

Figure 15. Cumulant U_L plotted versus temperature for $N = 576$, $\langle\rho\rangle = 0.30$ and several values of M_b.

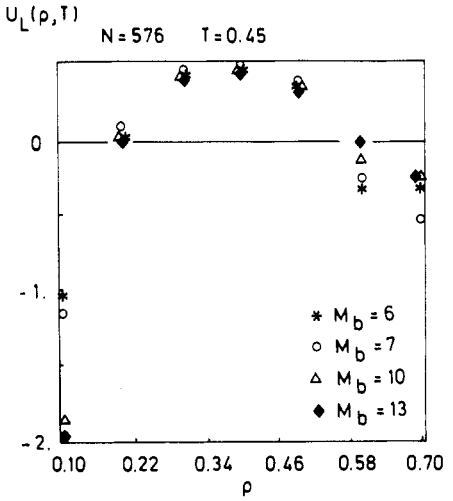

Figure 16. Cumulant U_L plotted versus density $\langle\rho\rangle$ for $N = 576$, $T = 0.45$ and $M_b = 6, 7, 10, 13$.

This implies that the dependence of U_L on the scaling variables $(\langle\rho\rangle - \rho_c)|\epsilon|^{-\beta}$ or $(\langle\rho\rangle - \rho_c)L^{\beta/\nu}$ in (25) and (29) is small. This implies for the analysis of section 2 that T_c can be estimated from the intersection of cumulants for different L (in a U_L versus T plot, figure 15), even if ρ_c is known only very imprecisely. We feel that $\rho_c = 0.30$ is probably an understimation of the critical density, because the intersection point in figure 15 occurs for $U^* \simeq 0.31$, i.e. distinctly below the expected universal value. But taking the evidence from figures 14 and 15 together, it seems plausible to conclude that

$$T_c = 0.50 \pm 0.02. \tag{34}$$

This estimate is in the range of the previous estimates given in the literature [13], but it is still not precise enough to warrant a finite-size scaling analysis where (24)–(29) are more thoroughly tested.

As a first check of the non-trivial variation of the cumulant with density (cf (23) and the comments thereafter), figure 16 gives some data for $N = 576$ at $T = 0.45$. As expected, the positive maximum of this curve occurs for a density not very far from the density $\rho \simeq 0.36$ of the rectilinear diameter, while near the coexistence curve U_L is large but negative.

6. Conclusions

The present investigation shows that ideas familiar from the computer simulation study of phase transitions and critical phenomena, such as subblock analysis and finite-size scaling, can be carried over to off-lattice problems such as critical phenomena and phase coexistence in the gas–liquid transition. However, it must be emphasised that our feasibility study shows that the problem is considerably more demanding in computational resources, and the data analysis is far more difficult.

In brief, the reasons for these difficulties are as follows:

(i) The updating step of the Monte Carlo procedure involves a lot of calculation in comparison with the simplistic Ising model, for which superfast algorithms implying special tricks such as multispin coding [36] can be implemented [37]. Since the program used here is necessarily several orders of magnitude slower, a calculation of 10^5 MCS/particle takes of the order of two hours of CRAY-XMP-48 time for $N = 576$; hence even modern vector computers do not yet allow the study of very large systems.

(ii) Using the canonical ensemble of a fluid, the finite-size properties are considerably more intricate than for the grand-canonical one. This fact is due to the complications involved by the two-phase coexistence, as analysed in section 2, whereas in a grand-canonical simulation one would always essentially stay in a pure phase. While for the lattice gas the use of grand-canonical ensemble poses no simulational problems whatsoever, the use of the grand-canonical ensemble for dense fluids still involves a lot of accuracy problems [6, 7, 9, 16].

(iii) While in the Ising lattice gas the critical density is $\rho_c = \frac{1}{2}$ because of particle–hole symmetry, it is not known for fluids in beforehand. Thus the $(T, \langle\rho\rangle)$ plane needs to be scanned in the simulation. In the Ising problem a single density ρ_c needs to be investigated.

(iv) Far away from the critical point, the Gibbs ensemble [19] can be used to estimate coexisting densities with relatively modest effort. However, the present method is believed to be advantageous in the critical region, where *finite-size effects must be considered*, which is possible with the methods presented here.

In view of all these problems, the extent to which our approach can be useful was not clear beforehand; therefore we have described the technical aspects and problems of such simulations in detail. We do feel, however, that the methods developed in the present paper are a useful approach for studying phase coexistence in fluids, including the vicinity of the critical point. As in the case of the lattice gas model, extremely small subsystems of medium size systems can yield good estimates of the densities of coexisting phases. Note that a single (but long!) simulation run yields information on all subsystem sizes simultaneously. The compressibility both in the one-phase region and at the coexistence curve also is an output of the calculation, though somewhat larger systems than studied here clearly are required for the desired accuracy. With a major effort of computing time it will be realistic to carry such a study to systems of a few thousand particles. Note that the subsystem analysis as described here can also be combined with a molecular dynamics simulation.

A meaningful study of critical point properties (critical exponents and amplitudes, etc.) still seems to be very difficult. We think that the present techniques should be useful for a rough estimation of phase diagrams, e.g., one could address the behaviour of various adsorbates on surfaces, where atoms also experience a periodic potential due to the substrate. Also the extension to three-dimensional systems is straighforward. We intend to report on such applications in future publications.

Acknowledgments

One of us (MR) gratefully acknowledges the fellowship from the von Humboldt Stiftung. We thank the Regionales Hochschulrechenzentrum Kaiserslautern for granting computer time on the Siemens–Fujitsu VP100 vector processor. The largest part of the computations was performed on the Cray XMP-48 of the Centro di Calcolo Elettronico Interuniversitario dell'Italia Nord Orientale under the SISSA–CINECA

joint project, sponsored by the Italian Ministry of Education. One of us (MR) would like to thank A Levi and A Parola for useful discussions.

Appendix. Predictions based on van der Waals theory

The free energy density according to van der Waals theory can be written as [27]

$$f_{vdw} = k_B T \rho \ln\left(\frac{\lambda^3 \rho}{e[1-\rho/(3\rho_c)]}\right) - \frac{9}{8} k_B T_c \frac{\rho^2}{\rho_c} \tag{A1}$$

where $\ln e = 1$, λ is the thermal de Broglie wavelength of the fluid atoms, and molecular parameters are eliminated in favour of the critical density ρ_c and critical temperature T_c. The corresponding pressure is

$$p = \frac{\rho k_B T}{[1-\rho/(3\rho_c)]} - \frac{9}{8} k_B T_c \frac{\rho^2}{\rho_c} \tag{A2}$$

and the isothermal compressibility K_T follows from

$$K_T^{-1} = \rho\left(\frac{\partial p}{\partial \rho}\right)_T = k_B T \rho\left[\left(1-\frac{\rho}{3\rho_c}\right)^{-2} - \frac{9}{4}\frac{T_c}{T}\frac{\rho}{\rho_c}\right]. \tag{A3}$$

From (A3) the estimate mentioned in table 3 is calculated, using $\rho = \rho_{liq}$ as given by the simulation, and $\rho_c = 0.3$. This yields $k_B T \rho_{liq} K_T^{liq} = 0.0526$ for $\rho_{liq} = 0.72$, while $\rho_{gas} = 0.021$ similarly implies $k_B T \rho_{gas} K_T^{gas} = 1.146$, whereas the ideal gas value would be $k_B T \rho_{ideal} K_T^{ideal} = 1$.

It is also instructive to recall the expansion of (A1) valid near T_c

$$f_{vdw} = f_0 + \mu_c(\rho-\rho_c) + \frac{9}{8} k_B T \rho_c \left(\frac{T}{T_c}-1\right)\left(\frac{\rho-\rho_c}{\rho_c}\right)^2 + \rho_c k_B T_c \frac{9}{64}\left(\frac{\rho-\rho_c}{\rho_c}\right)^4 + \cdots \tag{A4}$$

μ_c being the chemical potential at the critical point. The condition

$$\left(\frac{\partial f_{vdw}}{\partial \rho}\right)_{T,\rho_{liq}} = \mu_{liq} = \left(\frac{\partial f_{vdw}}{\partial \rho}\right)_{T,\rho_{gas}} = \mu_{gas}$$

implies that ρ_{gas} and ρ_{liq} are solutions of the equation

$$\frac{\mu-\mu_c}{k_B T_c \rho_c} = \frac{9}{4}\left(\frac{\rho-\rho_c}{\rho_c}\right)\left[\left(\frac{T}{T_c}-1\right) + \frac{1}{4}\left(\frac{\rho-\rho_c}{\rho_c}\right)^2\right]. \tag{A5}$$

For $\mu_{liq} = \mu_c$, $\mu_{gas} = \mu_c$, the coexistence curve is

$$\frac{\rho_{gas}-\rho_c}{\rho_c} = -2\sqrt{1-\frac{T}{T_c}} \qquad \frac{\rho_{liq}-\rho_c}{\rho_c} = +2\sqrt{1-\frac{T}{T_c}}. \tag{A6}$$

Using (A6) for $T/T_c = 0.9$ would yield $\rho_{gas} \simeq 0.10$, $\rho_{liq} \simeq 0.50$, which is distinctly off from the observed values. Using these estimates in (37) would yield $k_B T \rho_{liq} K_T^{liq} \simeq 1.116$, $k_B T \rho_{gas} K_T^{gas} \simeq 2.313$, instead of the estimates quoted above. This consideration shows that even for temperature 10% below T_c the van der Waals equation is a very imprecise description of two-dimensional Lennard-Jones fluids, which should be expected, of course.

Finally we note that the potential $g(T,\rho) = f(T,\rho) - \mu\rho$ entering $P_L(\rho)$ (cf (8)) can be written in the van der Waals approximation, using (4) and $\mu = \mu_c$

$$g_{vdw}(T,\rho) \simeq f_0 - \mu_c\rho_c + \frac{9}{64}k_B T_c \rho_c \left[-2\left(\frac{\rho_{gas}-\rho_c}{\rho_c}\right)^2\left(\frac{\rho-\rho_c}{\rho_c}\right)^2 + \left(\frac{\rho-\rho_c}{\rho_c}\right)^4\right] \quad \text{(A7)}$$

where we have used (A6) to eliminate $(T/T_c)-1$ via $-\frac{1}{4}[(\rho_{gas}-\rho_c)/\rho_c]^2$, as we consider densities near the gas branch. Equation (A7) can be written further as

$$g_{vdw}(T,\rho) \simeq f_0 - \mu_c\rho_c - \frac{9}{64}k_B T_c \rho_c \left[\left(\frac{\rho_{gas}-\rho_c}{\rho_c}\right)^4 - \left(\frac{\rho-\rho_{gas}}{\rho_c}\right)^2\left(\frac{\rho+\rho_{gas}-2\rho_c}{\rho_c}\right)^2\right]. \quad \text{(A8)}$$

For $\rho \simeq \rho_{gas}$ this is equivalent to

$$g_{vdw}(T,\rho) \simeq \text{constant} + \frac{9}{16}k_B T_c \rho_c \left(\frac{\rho_{gas}-\rho_c}{\rho_c}\right)^2\left(\frac{\rho-\rho_{gas}}{\rho_c}\right)^2 \quad \text{(A9)}$$

which is the form assumed in (14), and a similar expression is readily derived for ρ near ρ_{liq}. While (A9) implies a Curie–Weiss-like divergence of K_T^{liq}, K_T^{gas} along the coexistence curve, $K_T^{gas,liq} \propto (1-T/T_c)^{-1}$, as a comparison of (A9) and (A6) and (14) and (15) shows, we believe that (14) and (15) are more generally valid if the proper temperature dependence of ρ_{gas}, ρ_{liq}, K_T^{gas} and K_T^{liq} is used.

References

[1] Metropolis N, Rosenbluth A W, Rosenbluth M N, Teller A H and Teller E 1953 *J. Chem. Phys.* **21** 1087

[2] Alder B J and Wainwright T E 1957 *J. Chem. Phys.* **27** 1208

[3] Binder K (ed) 1979 *Monte Carlo Methods in Statistical Physics* (Berlin: Springer)

[4] Binder K (ed) 1984 *Applications of the Monte Carlo Methods in Statistical Physics* (Berlin: Springer)

[5] Binder K and Heermann D W 1988 *Monte Carlo Simulation in Statistical Physics—An Introduction* (Berlin: Springer)

[6] Heermann D W 1986 *Computer Simulation Methods in Theoretical Physics* (Berlin: Springer)

[7] Allen M P and Tildesley D J 1987 *Computer Simulations of Liquids* (Oxford: Clarendon)

[8] Ciccotti G and Hoover W G (ed) 1986 *Molecular Dynamic Simulations of Statistical Mechanical Systems* (Amsterdam: North-Holland)

[9] Ciccotti G, Frenkel D and McDonald I R (ed) 1987 *Simulation of Liquids and Solids* (Amsterdam: North-Holland)

[10] Hansen J P and Verlet L 1969 *Phys. Rev.* **184** 151

[11] Barker J A and Henderson D 1976 *Rev. Mod. Phys.* **48** 587

[12] Henderson D 1979 *Mol. Phys.* **34** 301

[13] Barker J A, Henderson D and Abraham F F 1981 *Physica* A **106** 226

[14] Adams J J 1979 *Mol. Phys.* **37** 211
[15] Ng K C, Valleau J P Torrie G M and Patey G N 1979 *Mol. Phys.* **38** 781
[16] Powles J G, Evans W A B and Quirke N 1982 *Mol. Phys.* **46** 1347
[17] Frenkel D 1986 *Molecular Dynamic Simulations of Statistical Mechanical Systems* ed G Ciccotti and W G Hoover (Amsterdam: North-Holland)
[18] Panagiatopoulos A Z, Suter U W and Reid R C 1986 *Ind. Eng. Chem. Fundam.* **25** 525
[19] Panagiatopoulos A Z 1987 *Mol. Phys.* **61** 813
Panagiatopoulos A Z, Quirke N, Stapleton M, and Tildesley D 1988 *Mol. Phys.* **63** 527
Smit B, de Smedt Ph and Frenkel D 1989 *Mol. Phys.* **68** 931
Smit B and Frenkel D 1989 *Mol. Phys.* **68** 951
[20] Strandburg K, Zellweg J A and Chester G V 1984 *Phys. Rev.* B **30** 2755
[21] Binder K 1981 *Z. Phys.* B **43** 119
[22] Kaski K, Binder K and Gunton J D 1984 *Phys. Rev.* B **29** 3996
[23] Binder K and Landau D P 1984 *Phys. Rev.* B **30** 1477
[24] For a general review of finite-size scaling near critical points, see Barber M N 1983 *Phase Transitions and Critical Phenomena* vol 8, ed C Domb and J L Lebowitz (New York: Academic) ch 2, and [25].
[25] Binder K 1987 *Ferroelectrics* **73** 43
[26] This was demonstrated for the first time in our preliminary report, Rovere M, Heermann D W and Binder K 1988 *Europhys. Lett.* **6** 585
[27] Landau L D and Lifshitz E M 1980 *Statistical Physics* 3rd edn (Oxford: Pergamon) part 1
[28] Challa M S S, Landau D P and Binder K 1986 *Phys. Rev.* B **34** 1841
[29] Katznelson E and Lauvers P G 1987 *Phys. Lett.* **B186** 385
[30] Peczak P and Landau D P 1989 *Phys. Rev.* B **39** 11932
[31] Furukawa H and Binder K 1982 *Phys. Rev.* A **26** 556
[32] The van der Waals equation is forced to pass through the *real* critical point. If one allows the equation to have a higher critical temperature, one would probably get a better agreement far from the critical point.
[33] Glandt E D 1978 *J. Chem. Phys.* **68** 2952
[34] Reddy M R and O'Shea S F 1986 *Can. J. Phys.* **64** 677
[35] Note that this universal value even for the Ising model could be estimated with a relative error of several per cent only. The number quoted is taken from [21] for $d = 3$ obtained $U^* = 0.27$, while the later more accurate study of the same model [22] yielded $U^* = 0.31$.
[36] See e.g. Wansleben S, Zabolitzky J and Kalle C 1984 *J. Stat. Phys.* **37** 283
[37] The fastest Ising program in $d = 3$ dimensions updates 847 million spins per second (Ito N and Kanada Y 1988 *Supercomputers* **5** 31). Other very fast programs are described by Bhanot G, Duke D and Salvador R 1986 *J. Stat. Phys.* **44** 985, and by Wansleben S 1987 *Comput. Phys. Commun.* **43** 315, for instance.